Effect of dasatinib against thyroid cancer cell lines *in vitro* and a xenograft model *in vivo*

D. CHAN[1*], J.W. TYNER[2*], W.J. CHNG[1,3], C. BI[3], R. OKAMOTO[4], J. SAID[5], B.D. NGAN[5], G.D. BRAUNSTEIN[4] and H.P. KOEFFLER[1,3,4]

[1]Department of Haematology-Oncology, National University Hospital, Republic of Singapore; [2]Oregon Health and Science University, Portland, OR, USA; [3]Cancer Science Institute, National University of Singapore, Republic of Singapore; [4]Department of Medicine, Cedars-Sinai Medical Center; [5]Department of Pathology, UCLA, Los Angeles, CA, USA

Received January 2, 2012; Accepted January 18, 2012

DOI: 10.3892/ol.2012.579

Abstract. Tyrosine kinase inhibitors (TKIs) have emerged as a promising class of agents against thyroid cancer. The aim of the present study was to investigate the *in vitro* and *in vivo* activity of dasatinib against a panel of thyroid cancer cell lines and explore possible mechanisms of action, using various assays and western blotting. Our results showed that dasatinib exhibits prominent cytostatic activity both *in vitro* and *in vivo* against thyroid cancer cell lines with RET/PTC rearrangement (BHP2-7) and KRAS mutation (Cal62). Although dasatinib has primarily been described as an ABL/SRCfamily kinase inhibitor, the cytostatic activity observed in the present study is mediated by several off-target effects of dasatinib, some of which have not previously been reported. These effects include a reduction in phospho-FAK, FAK, RAS, Caveolin and SYK protein levels and an increase in β-catenin protein expression, which leads to the induction of senescence, an increase in the adhesiveness of the cells, a decrease in reactive oxygen species level, and changes in the expression profile of molecules involved in cellular adhesion such as integrins. Therefore, we propose that dasatinib is an effective therapeutic agent for certain patients with thyroid cancer, and these candidate patients may be identifiable on the basis of standard genotypic analyses.

Introduction

Radioiodine-resistant thyroid cancer remains a significant clinical challenge in spite of the advent of several small molecule tyrosine kinase inhibitors (TKIs) (1-4). Although BRAF is the most common mutation in papillary thyroid cancers, this is not the case in poorly differentiated and anaplastic thyroid cancers (5) where other genes such as RAS are equally/more important. A comprehensive study of thyroid cancer cell lines determined the validity of these cell lines, with some being confirmed as bona fide thyroid cancer cell lines, while others were either duplicate cell lines or established from non-thyroid tissue (6). This knowledge has enabled more recent *in vitro* studies of new agents against thyroid cancers to stratify the activity of these agents by the mutational composition of the cell lines (e.g., BRAF and KRAS) (7).

By taking advantage of the knowledge gleaned from these previous studies, we now report the *in vitro* activity of dasatinib on 9 validated human thyroid cancer cell lines. As with many of the other TKIs that have been tested, dasatinib was active *in vitro* against only 2 of the 9 cell lines. However, this result was particularly notable, because dasatinib could be shown to exert potent cytostatic effect on the RET/PTC rearrangement (papillary thyroid cancer) and KRAS mutant (anaplastic thyroid cancer) cell lines (BHP2-7 and Cal62, respectively) through G1 arrest and senescence. Dasatinib also potently affected the pFAK/FAK, RAS, pERK/ERK, SYK, β-catenin and Caveolin signalling pathways in these two thyroid cancer cell lines. Microarray analysis further suggested that cell adhesion and integrin-related pathways were modulated by dasatinib. These *in vitro* results were confirmed in a murine xenograft model of Cal62, the more aggressive cell line of the two cell lines.

Materials and methods

Cells and reagents. BHP2-7 (RET/ PTC rearrangement), Cal62 (KRAS G12R mutant), SW1736 (BRAF mutant), ATC238 (PI3K and BRAF mutant), Hth7 (NRAS Q61R), ATC241 (no mutation), ATC351 (no mutation), C643 (HRAS G13R) and Hth83 (HRAS G13R) cell lines were a generous gift from Dr James A. Fagin (Memorial Sloan Kettering Cancer Center, NY). Cells were grown and maintained in RPMI medium (Invitrogen, Carlsbad, CA, USA) containing 10% fetal bovine serum (Hyclone, Logan, UT, USA), 1% penicillin-streptomycin, and 1% glutamine at 37˚C with 5% CO_2 with

Correspondence to: Dr D. Chan, Department of Haematology-Oncology, National University Hospital Singapore, NUHS Tower Block, 1E Kent Ridge Road, Singapore 119228, Republic of Singapore
E-mail: daniel_chan@nuhs.edu.sg

*Contributed equally

Key words: senescence, migration, targeted therapy

the exceptions of SW1736 (additional 1% MEM non-essential amino acids to above) and Hth7 (DMEM instead of RPMI in the above). A stock solution of 10 mM of dasatinib (LC Laboratories, Woburn, MA, USA) was prepared using DMSO and stored at -20˚C. *In vitro* doses ranged from 0 to 10 μM.

Antibodies to RAS, phospho-FAK (Y576/Y577), GAPDH, Caveolin, SYK, β-catenin and ERK were obtained from Cell Signaling Technology (Boston, MA, USA). Antibodies to FAK and phospho-ERK were obtained from Santa Cruz Biotechnology (Santa Cruz, CA, USA).

High-throughput kinase inhibitor array assay. Thyroid cancer-derived cell lines were plated in 96-well plates at a seeding density of 1,000 cells per well over graded concentrations of 19 small-molecule kinase inhibitors. Each inhibitor was plated individually at four concentrations predicted to bracket the IC_{50} for that drug (in particular for dasatinib: 1, 10, 100 and 1000 nM). Cells were cultured in RPMI supplemented with 10% FBS, L-glutamine and penicillin/streptomycin (Invitrogen), and 10^{-4} M 2-mercaptoethanol (Sigma, St. Louis, MO, USA) for 72 h. At the end of the 72-h incubation, cell viability was assessed using the Cell Titer 96 Aqueous One Solution Cell Proliferation Assay (Promega, Madison, WI, USA). The values were normalized to the mean of seven wells on each plate containing no drug. The drug concentration at which growth is inhibited by 50% (IC_{50}) for each drug was then determined by identification of the two concentrations bracketing the 50% cell viability value and application of the following formula: [((A-50)/(A-B))*(Dose B-Dose A)]+Dose A where cell viability value >50% = A (drug dose for this value is Dose A) and cell viability value <50% = B (drug dose for this value is Dose B).

Cytotoxicity assay. Cells were plated in 96-well (Corning, Lowell, MA, USA) flat-bottomed microtiter plates at a concentration of 1000-5000 cells per well in 90 μl of medium. After overnight incubation at 37˚C, cells were treated with increasing concentrations of either dasatinib or vehicle (0.1% DMSO) and incubated for 72 h. After 72 h, 250 μg 3-(4,5-dimethylthiazol-2-yl)-2,5-diphenyltetrazolium bromide (MTT) (Sigma-Aldrich) was added to each well and incubated at 37˚C for 2-4 h. The 3-(4,5-dimethylthiazol-2-yl)-2,5-diphenyltetrazolium bromide was converted to formazan crystals by the mitochondria of the viable cells, which were then dissolved in 100 μl of DMSO. Absorbance was measured at 595 nm using a Tecan Infinite 200 PRO spectrophotometer (Mannedorf, Switzerland). Percentage viability at each drug concentration was calculated using the formula: (Absorbance of drug-treated cells - Absorbance of media only)/ (Absorbance of vehicle-treated cells - Absorbance of media only). The calculated percentage viability of cells at each (log_{10}) drug concentration was then plotted using GraphPad Prism® software non-linear regression (curve fit) to obtain the IC_{50} and its 95% confidence interval (CI).

For cell counting by trypan blue exclusion (at 24, 48 and 72 h), cells were grown in the appropriate media plus dasatinib for up to 72 h, collected by scraping (at each of the above time points), diluted in trypan blue dye (Sigma-Aldrich), and counted with a Brightline hemocytometer (Hausser Scientific, Horsham, PA, USA).

Cell migration assay and the scratch test. Cells were serum-starved overnight before the assay. Twelve-well plates with 8 μm polycarbonate membrane inserts (Millipore, Billerica, MA, USA) were used for the assay. Cells were harvested and suspended in serum-free medium at a concentration of $1x10^6$/ml. Cells were then incubated with 100 nM of dasatinib for 4 h at 37˚C. Cell suspension, 400 μl, was added to the inner chamber of the insert; serum-rich medium (1950 μl) was added to the outer chamber and the plates were incubated for 24 h. After 24 h, the chambers were removed, and the inner surface of the inserts was swabbed with cotton-tipped applicators to remove the cells that did not migrate. The outer surface of the inserts was then immersed in 50% crystal violet/50% methanol solution (Sigma-Aldrich) for 20 min. Excess crystal violet stain was carefully washed off using distilled water. The amount of crystal violet was photographed and quantified using an Optical Density (OD) 540 nm reading on a Tecan plate reader after dissolving with DMSO.

Random migration was also measured by the scratch test assay, in which cells were grown to 80% confluency in 6-well plates, streaked with a 1000 μl sterile pipette tip, and allowed to recover in dasatinib-treated media (100 nM). The plates were visualized at x4 (photography) and x10 (counting) magnification at various time points. Migration was determined by counting the number of cells migrated into the scratch using a microscope (Nikon Instruments Inc., NY, USA) at the 24-h mark. The assay was performed in triplicate and the number of migrated cells is expressed as a mean ± SD.

Western blotting. Proteins were collected from the cells grown in liquid culture treated with either vehicle or dasatinib (100 nM) for 48 h. Cells were washed in PBS and lysed at 4˚C in radio immunoprecipitation assay (RIPA) lysis buffer. Insoluble material was cleared by centrifugation at 4˚C 10000 g for 10 min. Protein was quantitated using Bradford reagent and BSA standard curve (Pierce, Rockford, IL, USA). Protein, 40 μg, from each sample was resolved by SDS-PAGE and transferred to Immobilon-P Transfer Membranes (Millipore). The membranes were blocked with 5% milk in TBS-Tween 20 and incubated with various primary antibodies overnight at 4˚C. Horseradish peroxidase-conjugated anti-rabbit/anti-mouse secondary antibody (Cell Signaling Technology) was used to detect protein-bound primary antibody. Bound secondary antibody was detected by using Amersham ECL Plus western blotting detection reagents (GE Healthcare, USA). Membranes were stripped for 30 min at 37˚C using stripping buffer (Pierce), reblocked, and probed for either GAPDH or the non-phosphorylated protein being analysed as loading controls.

Cell cycle analysis. Cell cycle distribution was analysed by plating cells at $3-4x10^5$ cells per 10 cm culture dish with complete medium at 24 h prior to treatment. Cells were exposed to vehicle (0.1% DMSO) or dasatinib (100 nM) for 72 h, collected, fixed in 70% ethanol, washed, and stained with a 5% propidium iodide solution. Samples were detected with a FACSCalibur (Becton-Dickinson, Franklin Lakes, NJ, USA) and analysed with FlowJo software (Tree Star Inc., Ashland, OR, USA).

Gene expression profiling and analysis. The mRNA expression was profiled in biological duplicates (Cal62 control or

Cal62 treated with dasatinib (100 nM, 30 h treatment), using Affymetrix Human Gene 1.0ST array (Affymetrix, Santa Clara, CA, USA) according to the manufacturer's protocol. Briefly, 200 ng of total RNA were reverse transcribed, amplified and labelled using Affymetrix Whole Transcript Sense Target Labelling and control reagents kit (Affymetrix), and then hybridized onto Human Gene 1.0ST array for 16 h at 60 rpm in a GeneChip Hybridization Oven 640 (Affymetrix). The arrays were washed using GeneChip Fluidics station 450 and scanned using GeneChip Scanner 3000 7G as per the manufacturer's instructions. The CEL files were imported into GeneSpring Software V11 for data normalization and identification of differentially expressed mRNAs of interest. Briefly, the CEL files were preprocessed using RMA16 algorithm and CORE transcript level. The data were then quantile normalized and those expression values less than the twentieth percentile were filtered out. Differentially expressed mRNAs of interest were identified using the fold-change function. Heatmaps were generated using the hierarchical clustering function. Gene ontology analysis was performed using the GO function.

In addition, to understand further the functional and biological relevance of differentially expressed genes, gene ontology and pathway/network analysis was performed using a web-based software, MetaCore (GeneGo, St. Joseph, MI, USA). The software contains an interactive, manually annotated database derived from literature publications on proteins and small molecules that allows for representation of biologic functionality and integration of functional, molecular, and clinical information. Several algorithms to enable both the construction and analysis of gene networks were integrated as previously described (8). The output P-values reflect scoring, prioritization, and statistical significance of networks according to the relevance of input data.

Apoptosis assay. Cells were treated with 100 nM of dasatinib for 72 h and labelled with FITC-conjugated Annexin V antibody and propidium iodide using Annexin V-FITC apoptosis detection kit I (BD Biosciences, San Jose, USA), according to the manufacturer's instructions. Positive cells were detected by fluorescence-activated cell sorting.

Senescence assay. Senescence assay was performed using the Cell Biolabs Inc. (San Diego, CA, USA) assay kit. Briefly, cells were incubated with 100 nM of dasatinib for 72 h prior to staining with SA-Beta-Galactosidase as per the manufacturer's instructions. Senescent cells (stained blue-green) were photographed under x20 magnification (Nikon, Japan) and counted under five random x10 high power field (hpf) for quantification. The average number and SD of the number of senescent cells per hpf was calculated. The quantitation was repeated in triplicates.

Reactive oxygen species assay. The reactive oxygen species (ROS) assay was performed using a kit from Cell Biolabs Inc. (San Diego). The standard curve was created using a serially-diluted (0, 0.039, 0.078, 0.156, 0.313, 0.625, 1.25, 2.5, 5, 10 and 20 μM) hydrogen peroxide solution supplied by the kit. The assay was performed at the 24-h time point which had been previously verified not to cause apoptosis or necrosis of the cells. The cells ($1x10^7$ per assay) were counted just prior to the ROS assay to ensure equal numbers in each group. The excitation wavelength (480 nm) and absorbance wavelength (530 nm) were measured with a Tecan Infinite 200 PRO spectrophotometer. The mean ROS levels of control and dasatinib-treated cells were compared using the Student's t-test to assess for statistical significance.

Murine studies. Six-week old female athymic nu/nu mice, NCRFU (Taconic Hudson, NY, USA) were fed *ad libitum* and kept in optimal hygienic conditions in a 12-h light/dark cycle. Upon arrival, animals were kept in the animal facility for a 1-week quarantine before starting the experiments. Mice were anaesthetized with inhalational Isoflurane (Hospira Lakeforest, IL). Cal62 cells ($1x10^6$) were resuspended in 50 μl Matrigel® (BD Biosciences) and 50 μl PBS for each tumor. Cells were injected subcutaneously on both flanks of the immunodeficient mice. A total of 20 tumors were inoculated (10 in the control and 10 in the drug treatment mice). The mice were administered either vehicle or dasatinib 12.5 mg/kg IP injection/day for 5 days/ week for 3 weeks at a 1:1 randomization ratio. The weight of the mice was measured every week.

At the end of either drug or vehicle-only treatment (35 days after tumor cell injection), the animals were sacrificed by CO_2 inhalation, tumor masses collected and volumes calculated according to the formula: (length x width x thickness x 0.5236). Measurements were made in millimetres using vernier callipers. A sample of the tissue was formalin-fixed for histological and immunohistochemical (IHC) analyses.

The murine studies were approved by the Animal Care and Use Committee of Cedars-Sinai Medical Center, and all animal care was in accordance with the IACUC guidelines. The mean weight of the tumor xenografts on Day 35 of the two groups was compared using the Student's t-test for statistical significance.

Results

Dasatinib reduces thyroid cancer cell viability in vitro in 2 of 9 cell lines at a pharmacologically achievable dose and is primarily cytostatic. To identify candidate small-molecule kinase inhibitors that were effective at reducing the growth of thyroid cancer cells, we performed a high-throughput screen to determine the IC_{50} values for 9 thyroid cancer cell lines across 19 small-molecule kinase inhibitors. This technique indicated that four cell lines (BHP2-7, Cal62, ATC351 and C643) (Fig. 1A) were relatively sensitive to dasatinib. The high-throughput kinase inhibitor assay screen IC_{50} results (Table I) were verified by MTT assay using more drug doses and time points (24, 48 and 96 h) in addition to the 72-h time point of the high-throughput kinase-inhibitor assay. BHP 2-7, the only RET/PTC rearrangement papillary thyroid cancer cell line, and Cal62, the only KRAS G12R mutant, were confirmed to be sensitive to dasatinib within a pharmacologically relevant dose of not more than 100 nM (Fig. 1B). The 72-h time point was the most reliable in assessing the efficacy of dasatinib on the viability of treated cells (data not shown).

Cell counting by trypan blue exclusion showed that the reduction in viability was mainly due to a cytostatic effect as the number of cells in the vehicle- and dasatinib-treated groups continued to increase (up to the observed time point of

Table I. IC_{50} (nM) from high-throughput kinase inhibitor array screen on 9 thyroid cancer cell lines.

Inhibitor	ATC238	HTH83	BHP	C643	CAl62	SW1736	ATC241	HTH7	ATC351
Staurosporine	97	170	6	6	6	8	522	61	9
PKC412	10000	10000	1012	875	1429	1610	10000	4887	1666
MLN518	10000	10000	10000	8970	10000	10000	10000	10000	10000
AST-487	4898	6481	523	2271	997	5099	5566	4811	5046
CHIR-258	5042	6375	544	3784	1201	4920	6028	4539	8968
Imatinib	10000	10000	10000	10000	10000	10000	10000	10000	10000
Nilotinib	10000	10000	8925	10000	8523	10000	10000	10000	10000
Dasatinib	1000	1000	294	377	716	1000	982	1000	587
AP24534	691	739	537	703	664	605	853	846	688
ZD-6474	5908	7700	4176	5627	430	10000	6560	4812	4783
Sunitinib	1000	1000	866	1000	1000	1000	1000	1000	1000
SU-14813	10000	10000	6363	10000	10000	10000	10000	6912	10000
Sorafenib	6460	7891	4991	6531	6377	10000	7436	6779	970
PTK787	10000	10000	10000	10000	10000	10000	10000	10000	10000
GW-786034	10000	10000	5585	8858	4948	10000	6680	10000	10000
AMG-706	10000	10000	10000	10000	10000	10000	10000	10000	10000
ABT-869	7716	10000	6725	6918	6507	10000	6243	5092	849
CHIR-265	10000	10000	82	6960	184	10000	10000	6978	10000
GW-2580	10000	10000	10000	10000	10000	10000	10000	10000	10000

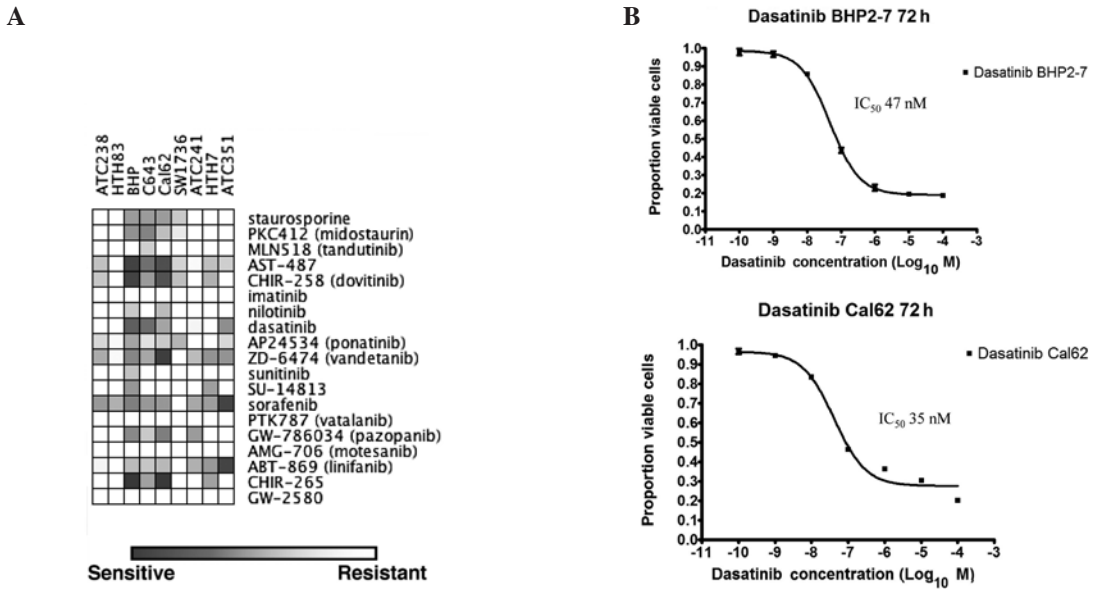

Figure 1. (A) High-throughput kinase-inhibitor array against a panel of 9 thyroid cancer cell lines is shown, with the cell lines listed at the top and various drugs listed on the vertical axis. The intensity of the gray boxes is directly proportional to the levels of growth inhibition of the particular cell line to the referenced drug. The white boxes indicate no growth inhibition. (B) The MTT assay curves of dasatinib-treated BHP2-7 (top) and Cal62 (bottom) at 72 h. The IC_{50} was 47 nM [95% confidence interval (CI) 44-51 nM] and 35 nM (95% CI 22-55 nM), respectively. MTT assays were performed in triplicate and data points are the mean (black circle) ± SD (stems).

72 h), although the cell increase in the dasatinib-treated group occurred at a slower rate (data not shown). This observation is further supported by the absence of apoptosis/necrosis on Annexin V/PI at the 72-h time point (see below).

Dasatinib has no effect on apoptosis but instead causes significant G1 arrest, increased cell adhesion and senescence. To characterize the effects of dasatinib on these thyroid cancer cell lines, we assessed the rates of apoptosis and senescence, cell cycle distribution, and adhesion with and without dasatinib treatment. Annexin V/PI showed no evidence of either early or late apoptosis at even up to 72 h exposure to dasatinib (100 and 1000 nM; data not shown). Significant dasatinib-induced G0-G1 arrest with an accompanying decrease in the S-phase

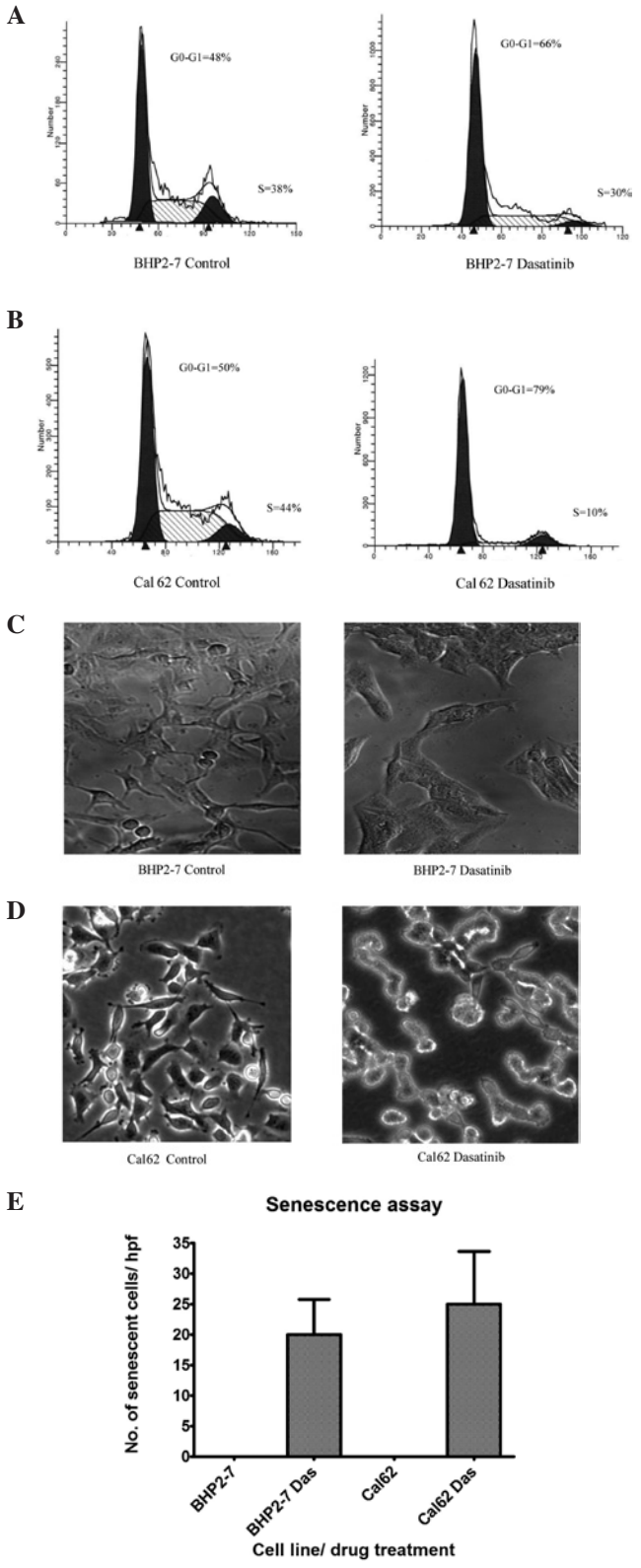

Figure 2. (A and B) Cell cycle analysis of BHP2-7 and Cal62 cells treated with vehicle control (left) or 100 nM dasatinib (right) for 72 h. The G0-G1 phase increased accompanying a decrease in the S-phase (BHP2-7 G0-G1 48 to 66%; Cal62 G0-G1 50 to 79%; BHP2-7 S-phase 38 to 30%; Cal62 S-phase 44 to 10%). (C and D) Microscope examination of BHP2-7 (x10) and Cal62 cells (x10) treated with either vehicle control (left) or 100 nM dasatinib (right). The untreated cells exhibited a dendritic morphology. Treatment with 100 nM of dasatinib for 72 h resulted in clumping of the cells (BHP2-7 and Cal62) and an altered clumped morphology (Cal62). (E) Detection of senescence by way of staining with SA-β galactosidase of dasatinib (100 nM, 72 h)-treated BHP2-7 and Cal62 cells. Senescent cells: 20 cells/hpf for dasatinib-treated BHP2-7 and 25/hpf for dasatinib-treated Cal62. hpf, high power field.

was noted in BHP2-7 (Fig. 2A) and Cal62 (Fig. 2B): BHP2-7, G0-G1 48 (control) to 66% (dasatinib); Cal62, G0-G1 50 (control) to 79% (dasatinib); BHP2-7, S-phase 38 (control) to 30% (dasatinib); Cal62, S-phase 44 (control) to 10% (dasatinib).

The dasatinib-treated (100 nM 72 h) BHP2-7 (Fig. 2C) and Cal62 (Fig. 2D) cells exhibited a characteristic clumped appearance; and most of these cells were verified (using a SA-β-Galactosidase assay) to be senescent. The average number of senescent cells per hpf was: BHP2-7, Control 0/hpf; BHP2-7, dasatinib (100 nM 72 h) 20/hpf; Cal62, Control 0/hpf; Cal62, dasatinib (100 nM 72 h) 25/hpf (Fig. 2E). Senescent cells were further monitored and were noted to become necrotic following 10 days of dasatinib treatment (data not shown).

Dasatinib inhibits thyroid cancer cell migration. The scratch test (Fig. 3A) and Boyden chamber assay (Fig. 3B) showed that 100 nM dasatinib inhibited migration of the thyroid cancer cell lines BHP2-7 and Cal62. The dasatinib-treated cells exhibited a nearly complete blockade in the ability to migrate across the polycarbonate insert; and even after 24 h were also unable to close the scratch whereas untreated cells were able to migrate better through the Boyden chamber, as well as randomly migrate across the scratch mark. Fig. 3A and B shows the quatitation of the degree of migration shown by the two assays.

Microarray analysis reveals the upregulation of genes related to cell/extra-cellular matrix adhesion in dasatinib-treated thyroid cancer. Out of 149 genes that are at least ≥2-fold upregulated, 8 of the genes are correlated with cell adhesion: Cadherin 6 (CDH6), ITGA11 (Integrin α11), Neuronal Cell Adhesion Molecule (NRCAM), Thrombospondin (THBS1), Integrin β3 (ITGB3), Fibrillin 1 (FBN1), Integrin β8 (ITGB8) and Tenascin C (TNC). Conversely, ITGA6 (the oncogenic integrin α6) was downregulated >2-fold.

Thyroid gland carcinomas have high levels of FAK and SYK mRNA and protein. Dasatinib inhibits Caveolin expression, Focal Adhesion Kinase (FAK), SYK, RAS and pERK (Fig. 4B and C). We initially assessed potential targets in thyroid cancer by examining mRNA expression data obtained from Oncomine® (USA) and found that the expression level of SYK and FAK (PTK2) were high in thyroid cancers relative to other types of cancer (Fig. 4A).

BHP2-7 and Cal62 cell lines treated with dasatinib 100 nM for 48 h had reduced total and phosphorylated FAK (Tyr 576/577), and decreased levels of SYK (Fig. 4B). Cells also had reduced RAS and Caveolin levels after exposure to dasatinib (Fig. 4C). Dasatinib caused a slight increase of (total) β-catenin in the Cal62 and BHP2-7 cell lines, but cellular localization was not determined (Fig. 4C).

Dasatinib reduces the level of reactive oxygen species in BHP2-7 and Cal62 cell lines. The two cell lines have high endogenous levels of reactive oxygen species (ROS); KRAS mutant Cal62 cells>RET mutant cells BHP2-7. To determine whether dasatinib has an impact on ROS levels, we treated cells with dasatinib and assayed the ROS levels. The ROS levels of the two cell lines were significantly reduced by dasatinib treatment (100 nM 24 h): Mean hydrogen peroxide concentration ± SD of BHP2-7: Control, 0.86 + 0.13 μM vs. dasat-

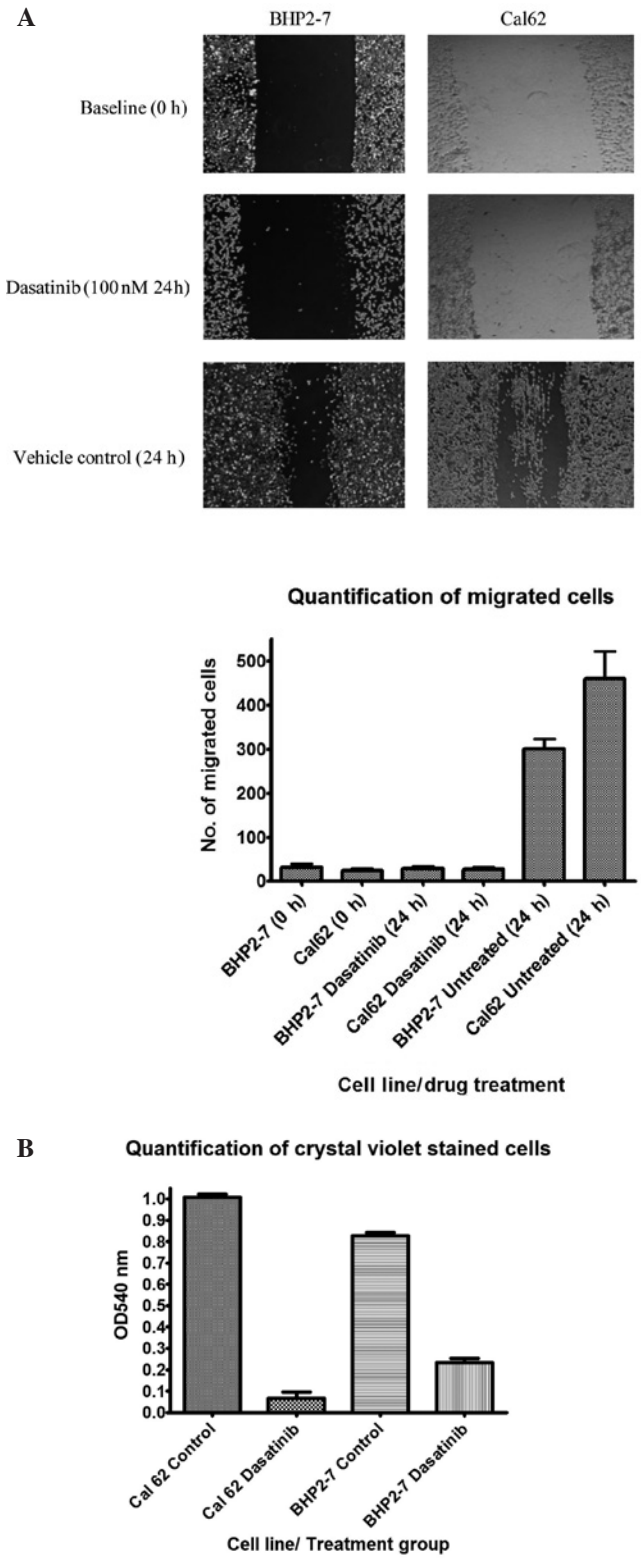

Figure 3. (A) Scratch test assay of Cal62 cell line treated with dasatinib (100 nM, 24 h) visualised under microscope. The baseline scratch mark defect created is shown in the top row. In contrast with vehicle (0.1% DMSO) treated BHP2-7 and Cal62 (bottom row), the dasatinib-treated cells (middle row) were unable to migrate across the defect created. Quantification of the number of cells migrated into the scratch defect at the 24-h mark is shown on the right (mean ± SD of triplicates). BHP2-7: 32±13 (Baseline), 29±8 (dasatinib-treated 24 h), 301±39 (vehicle-treated 24 h). Cal62: 25±7 (Baseline), 27±9 (dasatinib-treated 24 h), 461±107 (vehicle-treated 24 h). (B) The amount of migrated cells was indirectly quantified by measuring the optical density at 540 nm ($OD_{540\ nm}$) of the dissolved crystal violet. BHP2-7 $OD_{540\ nm}$ 0.827±0.027 (control), 0.233±0.035 (dasatinib); Cal62 1.007±0.024 (control), 0.066±0.053 (dasatinib).

inib-treated, 0.13 ± 0.03 μM ($p<0.05$ Student's t-test); Cal62: Control, 2.73 ± 0.55 μM vs dasatinib-treated, 0.59 ± 0.13 μM ($p<0.05$ Student's t-test).

Dasatinib inhibits KRAS mutant, anaplastic thyroid cancer cell line (Cal62) in vivo. To determine whether these *in vitro* effects of dasatinib could be recapitulated *in vivo*, we established a xenograft model of KRAS mutant, Cal62 cells, which are the more aggressive of the two dasatinib-sensitive cell lines. Treatment of mice with dasatinib (12.5 mg/kg IP injection/day for 5 days/week for 3 weeks) achieved a significant growth inhibitory effect on Cal62 thyroid cancer xenografts in our athymic mice model compared with the vehicle-treated mice (Fig. 6A). After an initial lag of 1-2 weeks, the tumor sizes of vehicle-treated controls increased at a faster rate than the tumors in the dasatinib-treated mice. The vehicle-treated tumors were approximately double in size and weight ($p<0.05$) compared to the dasatinib-treated tumors on Day 35 (Fig. 6B and C). Haematoxylin and eosin (H&E) staining of the tumors revealed prominent necrosis in tumors of the dasatinib-treated mice as compared to the vehicle-treated animals (Fig. 6D). Ki67 staining of the vehicle-treated mice tumors showed a high proliferative index (>75%) for this thyroid cancer cell line and that the dasatinib-treated mice tumors had a markedly lower Ki67 index (Fig. 6E).

Discussion

In recent years, various small molecule tyrosine kinase inhibitors including sorafenib, motesanib, pazopanib and axitinib in Phase II clinical trials (1-4) have shown modest activity in thyroid cancer (mainly stable disease by RECIST criteria) (9). However, the exact mechanism of action of these agents is uncertain, given the poor correlation between the predicted *in vitro* targets (e.g., RET and BRAF inhibitors) of these agents, mutational status of the tumors (RET and BRAF mutations) and clinical response (10). Of note, the RECIST clinical response rates of the above-mentioned kinases in clinical trials are all markedly similar in spite of the differences in spectrum of their kinase targets. Another possibility is that an as yet undiscovered stromal activity (including effects on cell adhesion and integrin pathway signalling) of the TKIs may be responsible for the cytostatic effect against thyroid cancer cells (as shown in our study) given the relatively poor direct cytotoxicity of the TKIs (and staurosporine: a pan-tyrosine kinase inhibitor) *in vitro* (Fig. 1A).

Although dasatinib has been studied in other solid tumors such as ovarian, lung, breast (11,12), the *in vitro* and *in vivo* effects of dasatinib on thyroid cancer have as yet not been published to the best of our knowledge. Of all the kinase inhibitors in our inhibitor array, dasatinib was the focus of the present study as it is already in clinical use for other indications and no previous reports exist on the activity of dasatinib despite the availability of studies on the activity of other similar inhibitors such as AZD0530 in thyroid cancer. In our study, dasatinib was active against only 2 of the 9 thyroid cancer cell lines. Although low, this frequency is fairly comparable to the other clinically tested kinases as shown in the tyrosine kinase high-throughput assay screen (e.g., AMG706/motesanib) and even staurosporine (Fig. 1A). Furthermore although compounds such as sorafenib

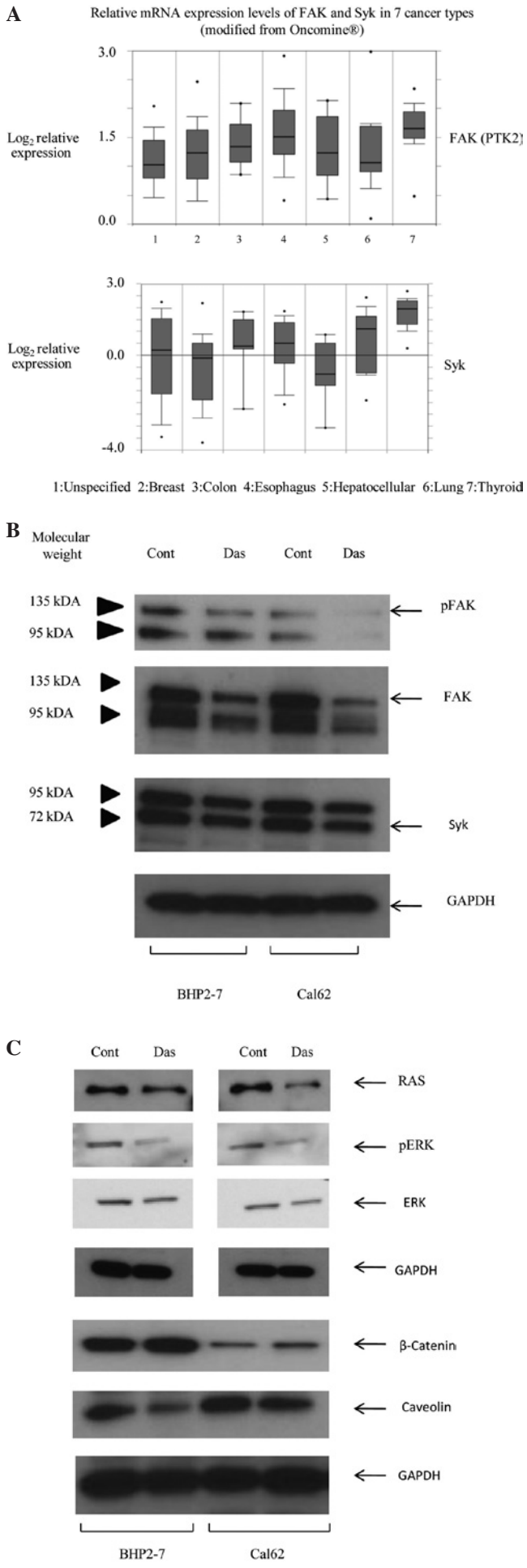

and vandetanib (ZD-6474) (Fig. 1A) exhibit anti-proliferative activity against most thyroid cancer cell lines in our kinase inhibitor array, their antiproliferative effects were observed only at levels of approximately 10 μM (a relatively high level). As such, the low pharmacologically achievable IC50 of <100 nM of dasatinib against the RET/PTC rearrangement (BHP2-7) and the KRAS mutant cell line (Cal62) in the *in vitro* studies and the murine study is noteworthy. Our finding of *in vitro* efficacy of dasatinib against a KRAS mutant anaplastic thyroid cancer cell line has not been previously noted.

Although BRAF is an important target in papillary thyroid cancer (13), reports are emerging that KRAS is an important target in anaplastic thyroid cancer (5). In addition, non-BCR-ABL dasatinib targets have been found for various tumor types. The role of the FAK pathway has recently been suggested to be important in PTC and ATC. Schweppe *et al* (14) characterized the antitumor effects of AZD0530, in PTC and ATC cells providing the first evidence that FAK is phosphorylated in a subset of PTC tumor samples (15,16). Our results showed that a different Tyrosine residue on FAK (Tyr 576/577) from that found in the study by Schweppe *et al* was phosphorylated in thyroid cancer (14).

A decrease in Caveolin expression has previously been reported to be a predictive biomarker for tumor response in other tumor types (17-19), thus our observation of Caveolin decrease after dasatinib treatment is a promising result. Along similar lines, it is of note that certain proteins known to be involved in cell adhesion-related intracellular signalling (i.e., FAK and Caveolin) are reduced in the two dasatinib-sensitive thyroid cancer cell lines. Caveolin-1 has RAS and ERK among its downstream effector proteins; the reduction in RAS and pERK are consistent with the observed decrease in Caveolin protein levels. FAK usually helps disassemble focal adhesions and the loss of adhesions is required for normal cell and cancer cell migration. Numerous cancer cells have elevated levels of FAK (Fig. 4A), which may explain their frequent motility as compared to their normal counterparts. As such, the dasatinib-induced reduction in pFAK and total FAK may help to explain the increased cell adhesion observed upon dasatinib treatment (20). The increase in mRNA expression of adhesion-related genes (CDH6, ITGA11, NRCAM, THBS1, ITGB3, FBN1, ITGB8 and TNC) and the decrease in mRNA of ITGA6 in dasatinib-treated Cal62 further supports the fact that dasatinib affects cell adhesion and the integrin pathway. ITGA6 (partner of Integrin α6β4 complex) is known to be an oncogenic integrin (21) among the large family of integrin molecules. It possesses, as its downstream targets, THBS1 (Thrombospondin 1) and TNC (Tenascin C), which are regulated in a negative feedback loop (22). As such, a corresponding increase in THBS1 and

Figure 4. (A) Modified data obtained from Oncomine showing high levels of FAK (PTK2) and SYK mRNA expression levels in various cancers. Y-axis shows relative Log_2 expression among the listed cancers. X-axis shows different cancer types. Thyroid cancer is labelled as '7'. (B and C) Western blots of the BHP2-7 and Cal62 cell lines are shown. Cells were treated with either vehicle (Cont) or dasatinib (Das) (100 nM, 48 h). Lysates were prepared for western blots which were probed for a variety of antibodies. (B) pFAK (Tyr576/577), total FAK and SYK levels. (C) RAS, Caveolin, pERK and total β-catenin levels and the molecular weight of pFAK/FAK (125 kDa) and Syk (80 kDa) are shown. The extra band in the pFAK, FAK and Syk blots (of the incorrect molecular weight) is a non-specific band.

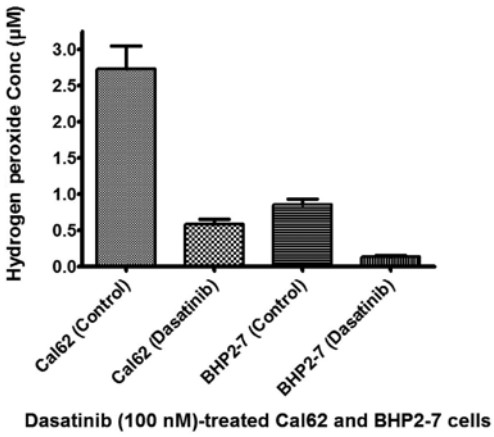

Figure 5. The effects of dasatinib on reactive oxygen species (ROS)/hydrogen peroxide levels in the BHP2-7 and Cal62 thyroid cancer cell lines is shown, as measured on a Tecan Infinite 200 PRO plate reader. Results show a reduction in the ROS levels with 100 nM of dasatinib treatment in BHP2-7 and Cal62 cell lines. Cal62, the more aggressive of the two cell lines, has higher basal levels of ROS than BHP2-7. The concentration of ROS in triplicate for BHP2-7 and Cal62 cell lines treated with either vehicle control or dasatinib was expressed as the mean ± SD. P<0.05 by the Student's t-test for control vs. dasatinib for the two cell lines.

TNC in parallel with the decrease in ITGA6 occurs. This observation is further supported by the KEGG analysis of the microarray data showing changes in cell adhesion-related genes (data not shown).

Although Syk has classically been associated with hematopoietic cells/malignancies, it is expressed in solid malignancies (including thyroid) (Fig. 4A: microarray data from Oncomine). At present, the data available on the role of Syk in solid malignancies remain unclear although it has paradoxically been reported to be a potential oncogene in ovarian cancer (23) and a tumor suppressor in breast cancer (24). Our finding that the Syk protein is highly expressed in thyroid cancer and is decreased by dasatinib treatment suggests it may be an oncogene in thyroid cancer.

Total β-catenin increased in the dasatinib-treated cells consistent with the microscopic findings of increased cell contact/adhesion with dasatinib treatment (Fig. 2C and D). Besides being involved in the Wnt signalling pathway, β-catenin is also part of a protein complex that constitutes adherent junctions. These junctions are necessary for the creation and maintenance of the integrity of epithelial cell layers by regulating cell growth and adhesion between cells. β-catenin also anchors the actin cytoskeleton and may be responsible for transmitting the contact inhibition signal that causes cells to stop dividing once the epithelial sheet is complete (25). As an example, β-catenin is expressed at low levels in metastatic gastric cancer (26). The increase in total β-catenin following dasatinib treatment may explain the observed increased adhesiveness of the two sensitive cell lines resulting in their impaired migration.

The majority of the TKIs, including the potent anti-BRAF TKI, PLX4032/PLX4720, are only cytostatic against thyroid cancer cell lines. The fact that these potent BRAF TKIs are ineffective against thyroid cancers with RET/PTC rearrangements or RAS mutants (27), emphasizes the clinical importance of the effectiveness of dasatinib against thyroid cancer cell lines carrying RET/PRC rearrangements or RAS mutations.

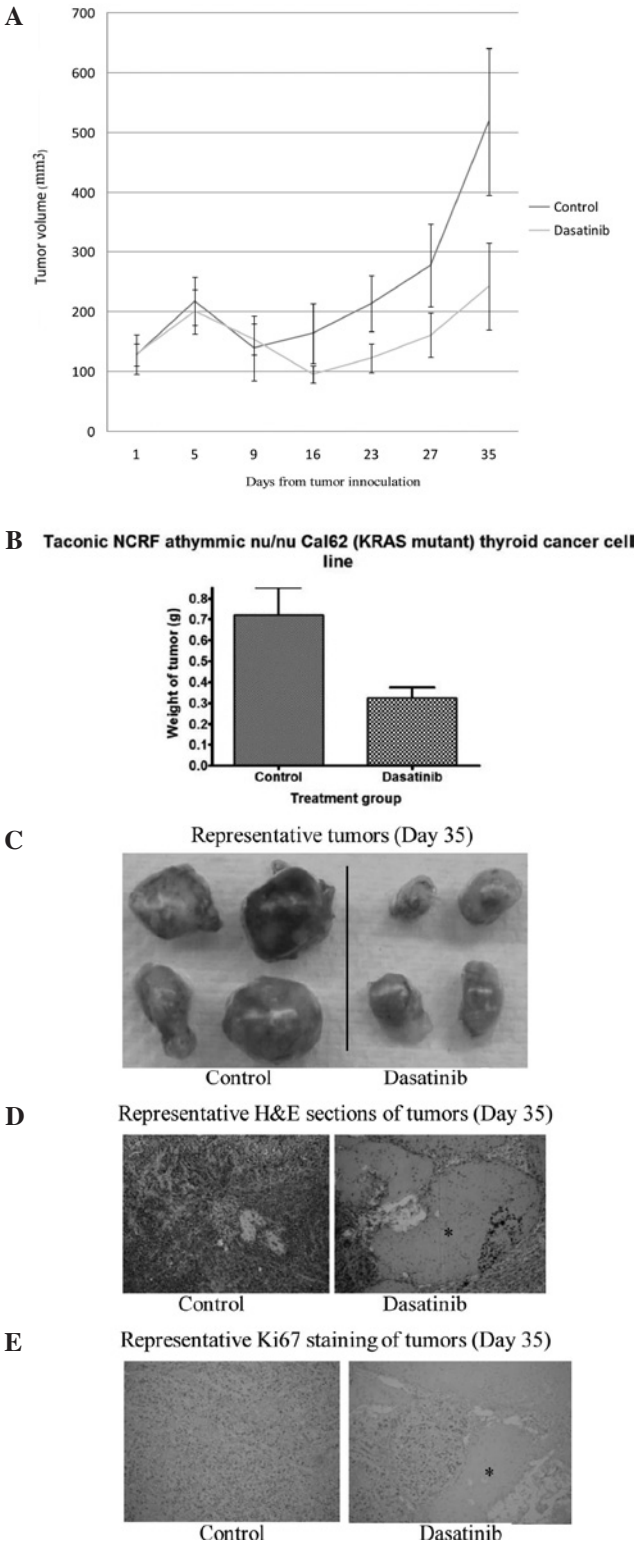

Figure 6. (A) Size of the Cal62 xenografts in athymic mice treated with vehicle or dasatinib as measured by vernier callipers and calculated using the formula: length x width x thickness x 0.5236, is shown. (B) Weight of the dissected tumors (in grams) on Day 35 from mice treated with dasatinib or vehicle for 3 weeks (5 days per week) (p<0.05 by Student's t-test) are noted. (C) Representative dissected tumors from vehicle-treated mice (left) and dasatinib-treated mice (right) show the difference in the size of the tumors. (D) Haematoxylin and eosin staining of formalin-fixed tumor specimens from the vehicle-and dasatinib-treated mice. *Typical area of prominent necrosis in the dasatinib-treated tumor, not observed in the tumor from the vehicle-treated mice. (E) Ki67 staining of the tumor specimen from either vehicle- or dasatinib-treated mice. Of note is the >75% Ki67 staining of cells of this extremely aggressive tumor in vehicle-treated mice. *Absence of Ki67 staining in the necrotic part of the dasatinib-treated tumor is shown.

Our findings have shown in the two dasatinib-sensitive thyroid cancer cell lines that senescence was a dominant process at the early time points of up to 72 h, as no necrosis or apoptosis occurred. Several pathways have been reported to mediate senescence including p53 and p21 (28,29), although upregulation of p21 was found in neither of these cell lines in our study. Additional treatment (up to 10 days) of the BHP2-7 and Cal62 cell lines with dasatinib resulted in necrosis. This finding is further supported by the observation that the dasatinib-treated xenograft tumors in the mice showed prominent necrosis at Day 35 post-innoculation of the tumors.

Earlier studies observed a correlation between the expression of oncogenes and cellular ROS levels, such as increased ROS production in response to RAS oncogenic activity in H-RASv12-transformed NIH3T3 fibroblasts (30). Further studies showed that the upregulation of RAS protein signalling through either overexpression or mutational activation were associated with increased ROS production, cell oxidative stress, and mutagenesis (30). Similarly, previous studies have shown the importance of ROS in thyroid disease pathophysiology (31,32). The high levels of ROS in Cal62 (KRAS mutant) and to a lesser extent in BHP2-7 (RET/ PTC rearrangement) (upstream of RAS) may be explained by the above observations.

In conclusion, we are the first to report prominent *in vitro* and *in vivo* activity of dasatinib against 2 thyroid cancer cell lines (RET/PTC rearrangement and KRAS mutant). Dasatinib caused cytostatic death by G1-arrest and senescence involving Syk, β-catenin, FAK, RAS, ERK and Caveolin. Dasatinib may thus be useful specifically in RET mutant papillary thyroid cancers and KRAS mutant anaplastic thyroid cancers. The findings of novel off-target effects of dasatinib, including the blunting of the oncogenic integrins/cell adhesion/cell adhesion-related intracellular signalling (e.g., FAK) are noteworthy and should also be explored as potential properties of other TKIs in view of their lack of direct cytotoxicity.

Acknowledgements

D. Chan was funded by a Singapore National Medical Research Council (NMRC) Overseas Research Fellowship 2010/2011.

References

1. Cohen EE, Rosen LS, Vokes EE, *et al*: Axitinib is an active treatment for all histologic subtypes of advanced thyroid cancer: results from a phase II study. J Clin Oncol 26: 4708-4713, 2008.
2. Gupta-Abramson V, Troxel AB, Nellore A, *et al*: Phase II trial of sorafenib in advanced thyroid cancer. J Clin Oncol 26: 4714-4719, 2008.
3. Sherman SI, Wirth LJ, Droz JP, *et al*: Motesanib diphosphate in progressive differentiated thyroid cancer. N Engl J Med 359: 31-42, 2008.
4. Bible KC, Suman VJ, Molina JR, *et al*: Efficacy of pazopanib in progressive, radioiodine-refractory, metastatic differentiated thyroid cancers: results of a phase 2 consortium study. Lancet Oncol 11: 962-972, 2010.
5. Nikiforov YE: Thyroid carcinoma: molecular pathways and therapeutic targets. Mod Pathol 21 Suppl 2: S37-S43, 2008.
6. Schweppe RE, Klopper JP, Korch C, *et al*: Deoxyribonucleic acid profiling analysis of 40 human thyroid cancer cell lines reveals cross-contamination resulting in cell line redundancy and misidentification. J Clin Endocrinol Metab 93: 4331-4341, 2008.
7. Smallridge RC, Marlow LA and Copland JA: Anaplastic thyroid cancer: molecular pathogenesis and emerging therapies. Endocr Relat Cancer 16: 17-44, 2009.
8. Ekins S, Nikolsky Y, Bugrim A, Kirillov E and Nikolskaya T: Pathway mapping tools for analysis of high content data. Methods Mol Biol 356: 319-350, 2007.
9. Cabanillas ME, Waguespack SG, Bronstein Y, *et al*: Treatment with tyrosine kinase inhibitors for patients with differentiated thyroid cancer: the M. D. Anderson experience. J Clin Endocrinol Metab 95: 2588-2595, 2010.
10. Licitra L, Locati LD, Greco A, Granata R and Bossi P: Multikinase inhibitors in thyroid cancer. Eur J Cancer 46: 1012-1018, 2010.
11. Konecny GE, Glas R, Dering J, *et al*: Activity of the multikinase inhibitor dasatinib against ovarian cancer cells. Br J Cancer 101: 1699-1708, 2009.
12. Vitali R, Mancini C, Cesi V, *et al*: Activity of tyrosine kinase inhibitor Dasatinib in neuroblastoma cells in vitro and in orthotopic mouse model. Int J Cancer 125: 2547-2555, 2009.
13. Frasca F, Nucera C, Pellegriti G, *et al*: BRAF(V600E) mutation and the biology of papillary thyroid cancer. Endocr Relat Cancer 15: 191-205, 2008.
14. Schweppe RE, Kerege AA, French JD, Sharma V, Grzywa RL and Haugen BR: Inhibition of Src with AZD0530 reveals the Src-Focal Adhesion kinase complex as a novel therapeutic target in papillary and anaplastic thyroid cancer. J Clin Endocrinol Metab 94: 2199-2203, 2009.
15. Caccia D, Micciche F, Cassinelli G, Mondellini P, Casalini P and Bongarzone I: Dasatinib reduces FAK phosphorylation increasing the effects of RPI-1 inhibition in a RET/PTC1-expressing cell line. Mol Cancer 9: 278, 2010.
16. McLean GW, Carragher NO, Avizienyte E, Evans J, Brunton VG and Frame MC: The role of focal-adhesion kinase in cancer - a new therapeutic opportunity. Nat Rev Cancer 5: 505-515, 2005.
17. Parton RG and Simons K: The multiple faces of caveolae. Nat Rev Mol Cell Biol 8: 185-194, 2007.
18. Wary KK, Mariotti A, Zurzolo C and Giancotti FG: A requirement for caveolin-1 and associated kinase Fyn in integrin signaling and anchorage-dependent cell growth. Cell 94: 625-634, 1998.
19. Huang F, Reeves K, Han X, *et al*: Identification of candidate molecular markers predicting sensitivity in solid tumors to dasatinib: rationale for patient selection. Cancer Res 67: 2226-2238, 2007.
20. Judson PL, He X, Cance WG and Van Le L: Overexpression of focal adhesion kinase, a protein tyrosine kinase, in ovarian carcinoma. Cancer 86: 1551-1556, 1999.
21. Chen M and O'Connor KL: Integrin alpha6beta4 promotes expression of autotaxin/ENPP2 autocrine motility factor in breast carcinoma cells. Oncogene 24: 5125-5130, 2005.
22. Chen M, Sinha M, Luxon BA, Bresnick AR and O'Connor KL: Integrin alpha6beta4 controls the expression of genes associated with cell motility, invasion, and metastasis, including S100A4/metastasin. J Biol Chem 284: 1484-1494, 2009.
23. Sultan A, Wang C, Duran G, Francisco E, Berek J and Sikic B: SYK inhibition results in increased sensitivity of OVCAR-3 cells to paclitaxel. AACR 2010: Abstract 3496, 2010.
24. Coopman PJ, Do MT, Barth M, *et al*: The Syk tyrosine kinase suppresses malignant growth of human breast cancer cells. Nature 406: 742-747, 2000.
25. Brembeck FH, Rosario M and Birchmeier W: Balancing cell adhesion and Wnt signaling, the key role of beta-catenin. Curr Opin Genet Dev 16: 51-59, 2006.
26. Ebert MP, Yu J, Hoffmann J, *et al*: Loss of beta-catenin expression in metastatic gastric cancer. J Clin Oncol 21: 1708-1714, 2003.
27. Salerno P, De Falco V, Tamburrino A, *et al*: Cytostatic activity of adenosine triphosphate-competitive kinase inhibitors in BRAF mutant thyroid carcinoma cells. J Clin Endocrinol Metab 95: 450-455, 2010.
28. Collado M, Blasco MA and Serrano M: Cellular senescence in cancer and aging. Cell 130: 223-233, 2007.
29. Latini FR, Hemerly JP, Oler G, Riggins GJ and Cerutti JM: Re-expression of ABI3-binding protein suppresses thyroid tumor growth by promoting senescence and inhibiting invasion. Endocr Relat Cancer 15: 787-799, 2008.
30. Hanahan D and Weinberg RA: Hallmarks of cancer: the next generation. Cell 144: 646-674, 2011.
31. Ha HC, Thiagalingam A, Nelkin BD and Casero RA Jr: Reactive oxygen species are critical for the growth and differentiation of medullary thyroid carcinoma cells. Clin Cancer Res 6: 3783-3787, 2000.
32. Song Y, Driessens N, Costa M, *et al*: Roles of hydrogen peroxide in thyroid physiology and disease. J Clin Endocrinol Metab 92: 3764-3773, 2007.